Science
AAAS

The Formation of Chondrules: Petrologic Tests of the Shock Wave Model

Harold C. Connolly, Jr., *et al.*

Science **280**, 62 (1998);
DOI: 10.1126/science.280.5360.62

The Formation of Chondrules: Petrologic Tests of the Shock Wave Model

Harold C. Connolly Jr. and Stanley G. Love

Chondrules are millimeter-sized rounded igneous rocks within chondritic meteorites. Their textures and fractionated mineral chemistries suggest that they formed by repeated, localized, brief (minutes to hours) melting of cold aggregates of mineral dust in the protoplanetary nebula. Astrophysical models of chondrule formation have been unable to explain the petrologically diverse nature of chondrites. However, a nebular shock wave model for chondrule formation agrees with many of the observed petrologic and geochemical properties of chondrules and shows how particles within the nebula are sorted by size and how rims around chondrules are formed. It also explains the volatile-rich nature of chondrule rims and the chondrite matrix.

Meteorites are classified into many types, of which the most common (~80%) are the chondrites (*1*). Chondrites are subdivided into three groups—ordinary, carbonaceous, and enstatite—of which the ordinary chondrites are the most abundant. The distinguishing feature of these meteorites (composing up to 85% of their mass) is the eponymous chondrules (millimeter-sized silicate spheroids) they contain (Fig. 1). Many chondrites have remained unaltered since their formation 4.6 billion years ago (*1*), preserving a chemical composition matching that of the sun, except for the most volatile elements (*1*, *2*). Unaltered chondrites are one source of evidence about the processes that operated in the protoplanetary nebula: the thin, flat, rotating disk of gas and dust from which the sun and planets coalesced.

One of the most enigmatic nebular processes is the one that produced the chondrules. Chondrules are igneous rocks, believed to have formed by the brief melting of solid mineral precursors, which were afterward accreted into meteorite parent bodies (asteroids). Many mechanisms for the formation of chondrules have been proposed, but few of them have been rigorously tested against the petrological and geochemical constraints developed from meteorite studies, and none is generally accepted (*3*, *4*). For over 100 years, identifying the mechanism of chondrule formation has remained a leading task in meteoritics and planetary science (*3*, *5*, *6*).

Here we review and expand on the nebular shock wave model of chondrule formation (*3*, *7*). We then review the textural and chemical characteristics of chondrules that provide the strongest constraints on any mechanism for their formation and try to reconcile these observations with the shock wave theory.

The Shock Wave Model

A shock wave is a sharp discontinuity between hot, compressed, high-speed gas (moving faster than the local speed of sound) and cooler, less dense, slower moving gas. Gas overrun by a shock wave is abruptly heated, compressed, and accelerated. We envision the shock as a thin flat surface (a plane) moving through an initially cool, quiet [turbulent velocities of $\lesssim$50 m s^{-1} (*8*)] nebula of gas and dust. For simplicity, we consider a normal shock traveling in a direction perpendicular to its front surface. We assume a cold background nebula temperature T_0 of 300 K. The ambient pressure of the nebula p_0 is 1.00×10^{-5} bars. We assume that the gas is ideal, diatomic molecular hydrogen [molecular mass $m = 3.34 \times 10^{-27}$ kg per molecule; ratio of specific heats $\gamma = 1.4$ (*9*)], so the gas molecule number density (n_0) is 3.7×10^{20} m^{-3} and the gas mass density (ρ_0) is 1.23×10^{-6} kg m^{-3}. The speed of sound (a) in the gas before the shock is given by $(\gamma k T_0/m)^{0.5}$, where k is the Boltzmann constant (1.38×10^{-23} J/K) and m is the mass of one molecule. It is convenient to express the shock velocity (v_s) in terms of its Mach number (M), the ratio v_s/a. Given T_0, $a = 1300$ m s^{-1}.

Given M and the ideal gas equation of state, analytical relations (*10*) govern the post-shock density, pressure, velocity, and temperature (ρ_1, p_1, v_1, and T_1) in the gas (Fig. 2). Temperature and density increase moderately behind the shock wave, whereas pressure increases significantly. For example, in an M 5 shock, pressure increases by a factor of 29, density by a factor of 5, and temperature by a factor of 5.8.

Solid particles are also affected by the shock wave. When a shock wave overruns them, particles suddenly find themselves in a blast of wind moving at several kilometers per second. Friction or drag from collisions of gas molecules heats the particles, as does thermal radiation from hot neighboring particles. Particles lose heat by radiation and evaporation (*7*, *11*). In addition to gas drag heating, particles can be heated radiatively and conductively by the hot post-shock gas [at 1740 K in the M = 5 example] until cooling begins (*7*) or a post-shock

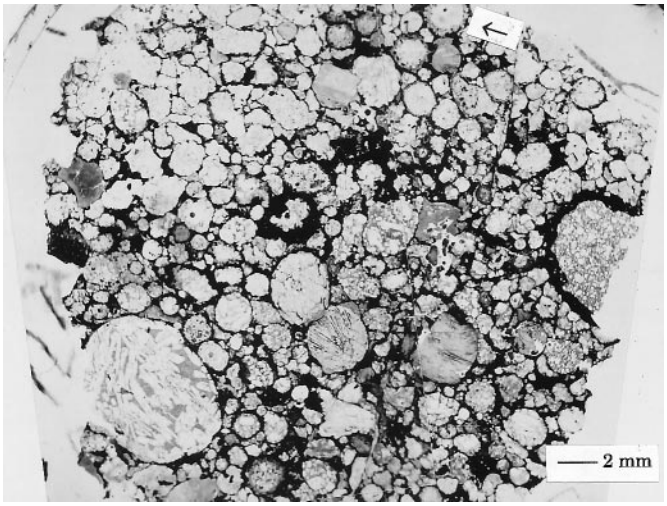

Fig. 1. A transmitted light image of a thin section of Semarkona (LL3.0; USNM 1805–4), an unequilibrated ordinary chondrite. This meteorite has experienced virtually no thermal metamorphism and thus contains chondrules that probably preserve a record of the preaccretional environment within the protoplanetary nebula. Note the diversity of the chondrules (the round objects) and their various sizes, shapes, and textures. The arrow marks a chondrule with an igneous rim.

H. C. Connolly Jr. is in the Division of Geological and Planetary Sciences, California Institute of Technology, Mail Code 100–23, Pasadena, CA 91125, USA. S. G. Love is at the Jet Propulsion Laboratory, Mail Code 306–438, 4800 Oak Grove Drive, Pasadena, CA 91109–8099, USA.

rarefaction wave (an "inverse shock" that cools and expands the gas) follows.

Once behind the shock, friction with the post-shock gas forces the particles to accelerate to match speeds with the gas. Drag heating ends when the particles attain the speed of the gas, which occurs when they have encountered a mass of gas comparable to their own mass. This corresponds to a distance behind the shock wave front on the order of the "stopping distance" $l_{stop} = d_p\rho_p/2\rho_g$, where d_p is the particle diameter, ρ_p is the particle density (2000 kg m^{-3} here for uncompacted silicate aggregates), and ρ_g is the post-shock gas density (6.15×10^{-6} kg m^{-3} for the M 5 example we give). Micrometer-sized particles attain the gas velocity within a few hundred meters of the shock wave, whereas millimeter-sized particles fall hundreds of kilometers behind the shock wave before matching speeds with the post-shock gas (Table 1). Thus, a transient region of size-sorted particles lies behind the shock front. Once particles of a given size come up to speed, their number density is concentrated by the same factor as the gas density (Fig. 3). Our drag heating calculations assume that the particles do not encounter a post-shock rarefraction wave before they match speeds with the gas. This in turn requires that the (as yet unidentified) source of the shocks have a time scale no shorter than the stopping time of the particles. For drag heating, the stopping time is equivalent to the heating duration. The shock source time scale is thus constrained by the inferred heating durations of chondrules.

Petrologic Observations and Their Relation to the Model

General petrology of chondrules. Chondrules have an igneous origin and are composed mainly of olivine [$(Mg,Fe)_2SiO_4$] and low-Ca pyroxene [$(Mg,Fe)_2Si_2O_6$] minerals set in a glassy-to-microcrystalline mesostasis (ground mass in which crystals are located) with varying minor amounts of Ca-rich pyroxene, Fe-rich metal, FeS, and spinel (*12*, *13*). The ferromagnesian chondrules are divided into groups based on their bulk compositions and textures: FeO-rich [bulk ~14 weight % FeO (Fig. 4A)] and FeO-poor [bulk ~2.5 weight % FeO (Fig. 4B)], which experienced slightly different formation conditions and can be found within the same meteorite (*5*, *6*, *13*, *14*).

Chondrule peak temperatures and cooling rates. The estimated peak melting temperatures, duration of melting, and cooling rates experienced by chondrules were derived from comparisons of textures and fractionated mineral chemistries (mainly variations in FeO and MgO contents of crystals) between synthetic and natural chondrules (*14*, *15*). Peak temperatures of chondrule formation range from 2000 to 2200 K for durations ranging from tens of seconds to several minutes (*3*, *5*, *6*, *13*–*15*). The lack of chemically homogeneous minerals within chondrules limits their cooling times from 30 min to a maximum of 2 days, although most chondrules appear to have cooled in ~2 to 5 hours (approximate linear cooling rates of 100° to 1000° per hour) (*3*, *5*, *6*, *15*, *16*). More prolonged heating would have facilitated elemental diffusion (equilibration) after crystallization (Fig. 4A) and recrystallized the glassy mesostasis (*13*, *15*). Although the diversity of chondrule compositions and textures prevents the unique determination of the temperatures and times of formation for all chondrules, the loss of volatile elements such as Na, K, Zn, and S (originally present in chondrule precursors) by evaporation during heating provides independent support for the range of temperatures, heating durations, and cooling rates derived from previous work (*17*, *18*).

Nebular shock waves of M 3 to 8 can heat initially cold chondrules to melting temperatures for times consistent with those determined experimentally (*7*) and produce post-shock cooling rates similar to those experienced by chondrules (*7*). Here we accept the heating duration and cooling rate calculations of previous studies (*7*, *8*, *19*), with one additional observation: A potential weakness of the shock wave model is that if shock waves stronger than M 8 occurred, they might have heated chondrules past their experimentally derived formation temperatures. This weakness disappears, however, because the maximum temperature of chondrule formation (2200 K) is similar to the temperatures at which molec-

Table 1. Drag heat pulse durations for different-sized particles in shocks of different strength.

M	1 μm	100 μm	300 μm	1 mm	2 mm	1 cm
4	55 ms	5.5 s	16.5 s	55 s	110 s	550 s
5	40 ms	4.0 s	12.0 s	40 s	80 s	400 s
6	32 ms	3.2 s	9.6 s	32 s	64 s	320 s
7	26 ms	2.6 s	7.8 s	26 s	52 s	260 s
8	22 ms	2.2 s	6.6 s	22 s	44 s	220 s

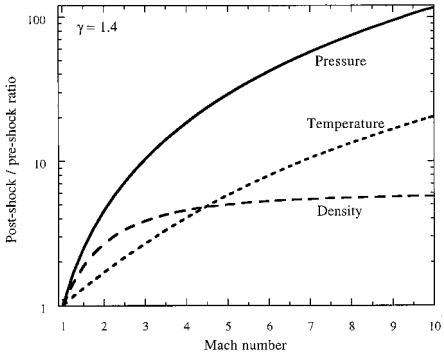

Fig. 2. Post- to pre-shock pressure, temperature, and gas density ratios as a function of shock strength expressed in M. Shocks of M 3 to 8 are thought to be capable of forming chondrules. An M 5 shock increases the density by factor of 5, the temperature by a factor of 5.8, and the pressure by a factor of 29.

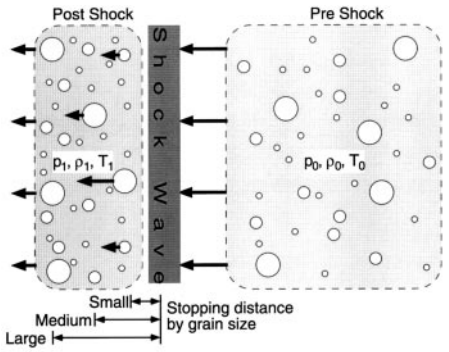

Fig. 3. Cartoon illustrating a shock wave in dusty gas, drawn from the perspective of an observer moving alongside the shock wave. Ambient nebular gas with pressure p_0, density ρ_0, and temperature T_0 enters the shock wave at the shock propagation speed v_s. The shock sharply (in the ideal case, instantaneously) compresses and heats the gas to higher pressure p_1, density ρ_1, and temperature T_1 while slowing its speed to v_1; the lost kinetic energy powers the heating and compression. Solid particles (which have random velocity very much smaller than the shock velocities) entering the shock abruptly find themselves in a hot high-pressure wind with velocity $(v_s - v_1)$. Collisions with gas molecules heat the particles while damping their velocity relative to the gas. Most of a particle's velocity is lost when it has penetrated one stopping distance ($l_{stop} = d_p\rho_p/2\rho_g$) past the shock front. The time scale of this process and of the gas drag heating pulse is $l_{stop}/(v_s - v_1)$. Small particles match speeds with the post-shock gas promptly (~200 m and ~0.05 s past the shock passage for a 1-μm grain in our "reference" M 5 shock). Larger particles take proportionally longer to come up to speed (for example, ~200 km and ~50 s for a 1-mm chondrule). A large particle suffers collisions with smaller grains moving at the speed of the gas just behind the shock. The final space density of solids (after matching speeds with the post-shock gas) is related to the pre-shock value by the same ratio as the gas density (ρ_1/ρ_0).

ular hydrogen dissociates and evaporative cooling begins (~2200 K) (*7*, *11*, *19*). These two processes absorb orders of magnitude more energy than simple caloric heating (*18*) and limit chondrule peak temperatures to the observed range even in shock waves substantially stronger than M 8.

Chondrule precursor temperatures. Some chondrule precursors (either pristine aggregates of minerals or previous generations of chondrules) were relatively cold before they were melted. Some FeO-poor (Fig. 4B) and small, fine-grained, dark-zoned (DZ) and agglomeratic olivine (AO) chondrules (Fig. 4C) of unaltered chondrites contain sulfides, predominantly FeS (*14*, *18*, *20*, *21*). The location of FeS within chondrules requires that it was part of their precursors and not an artifact of processes that occurred after the chondrules accreted onto asteroids (*14*, *18*, *20*, *21*). Because FeS has an evaporation temperature of ~648 K (*22*), the preservation of FeS in the FeO-poor, DZ, and AO chondrules requires that they were rapidly (minutes or less) heated to their peak melting temperatures from precursors that were resting at an ambient temperature of ≤648 K.

Solid carbon phases were also present in the protoplanetary nebula (*23*–*25*). The production of Fe-rich metal and its associated inclusions within many FeO-poor chondrules of carbonaceous chondrites requires one or more solid carbon phases to have been present within the precursor material (*24*) before melting. If this carbon resided in organic compounds (*23*), the ambient nebular temperature before the precursor material was melted to form chondrules could not have exceeded ~470 K without destroying these compounds.

The above constraints do not apply to FeO-rich chondrules, whose precursors contained neither solid carbon nor FeS (*12*, *13*). If present, carbon and FeS would have reacted with oxygen in the silicate melt to produce Fe-metal, which is not observed. However, FeO-rich chondrules contain higher abundances of moderately volatile elements such as Na and K as compared to FeO-poor chondrules (*5*, *6*, *12*–*14*). These elements evaporate at temperatures above ~970 K (*22*). Assuming that the majority of Na and K found in FeO-rich chondrules is retained from their precursors, those precursors could not have experienced temperatures in excess of ~970 K for more than a few minutes before melting (*12*, *17*).

Shock wave heating is consistent with the petrologic constraints on precursor temperature and heat pulse rise time (the time it takes for a particle's temperature to increase from that of the ambient nebula to

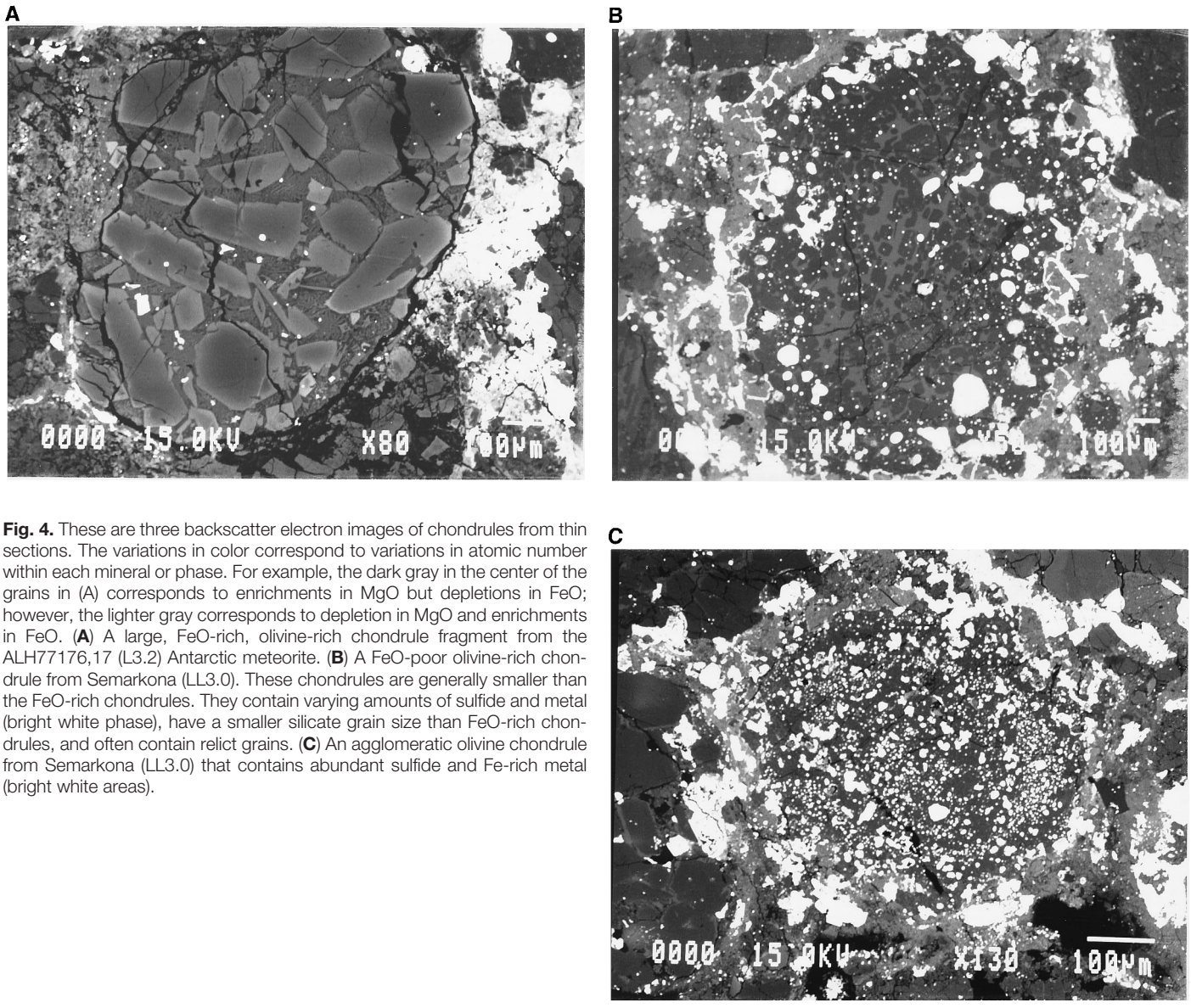

Fig. 4. These are three backscatter electron images of chondrules from thin sections. The variations in color correspond to variations in atomic number within each mineral or phase. For example, the dark gray in the center of the grains in (A) corresponds to enrichments in MgO but depletions in FeO; however, the lighter gray corresponds to depletion in MgO and enrichments in FeO. (**A**) A large, FeO-rich, olivine-rich chondrule fragment from the ALH77176,17 (L3.2) Antarctic meteorite. (**B**) A FeO-poor olivine-rich chondrule from Semarkona (LL3.0). These chondrules are generally smaller than the FeO-rich chondrules. They contain varying amounts of sulfide and metal (bright white phase), have a smaller silicate grain size than FeO-rich chondrules, and often contain relict grains. (**C**) An agglomeratic olivine chondrule from Semarkona (LL3.0) that contains abundant sulfide and Fe-rich metal (bright white areas).

peak heating temperature). Shock heating mechanisms such as conduction, collisions, and drag heating operate for any plausible pre-shock temperature. The shock heating rise time is almost instantaneous; particles are heated to their centers on time scales limited by their sizes and thermal diffusivities, ~1 s for 1-mm silicate spheres (*11*).

Chondrule recycling. Many chondrules contain relict grains (*12*, *13*, *26*) indicative of earlier generations of chondrules that were formed, broken, reaccreted, and remelted to form new chondrules (*12*, *13*, *26*, *27*). This observation requires that some chondrules experienced many episodes of heating, interspersed with epochs of fragmentation and accretion. Furthermore, the episodic heat pulses varied in intensity. Many chondrules have igneous rims (a rim of melted material similar in composition to the enclosed chondrule but preserving a distinct boundary between chondrule and rim), which accreted onto existing chondrules as fine-grained dust. Later or concurrent heating events melted these rims without melting the underlying chondrules (*28*).

Because shock waves need not be singular or identical events (*3*, *7*, *29*), they can provide the multiple heating episodes of varying intensity indicated by the texture and chemistry of some chondrules. If a shock wave passed through a region of the nebula traversed by earlier shock waves, existing chondrules would collide, break, and abrade behind the later wave as part of the recycling process.

In our shock wave model, a chondrule might collide with a particle half its size at half the post-shock gas speed, or ~2 km s^{-1} in the M 5 case. Such collisions would be relatively rare [assuming a common size spectrum for particles (*30*), in which most of the mass is contained in the smallest particles] but would break the chondrule into smaller fragments. This mechanism could create the chondrule fragments seen in some chondrites and potentially supply some of the relict grains observed in recycled chondrules (*12*, *13*, *26*, *31*).

Fine-grained dust and chondrule formation. Petrologic studies of chondrites suggest that chondrules formed in the presence of fine-grained dust, which is observed as chondrule accretionary (or fine-grained) rims and as fine-grained matrix material within unaltered meteorites, and is implicated as a seeding mechanism for the crystallization of some chondrules (*12*, *32*, *33*). This fine-grained rim and matrix material is richer in volatiles than are chondrules (*12*, *14*, *32*, *33*). The chemistries of chondrules and fine-grained material are complementary: Taken together, they approximate the solar composition except for the most volatile elements (*3*).

Shock wave heating can explain the accretion of rims on chondrules and the complementary relationship between rim and chondrule volatile chemistries. First, shock wave heating leads to high mutual velocities between particles of different sizes; recall that micrometer-sized grains stop within a few hundred meters of the shock front, where millimeter-sized chondrules have not slowed appreciably (Fig. 5A). The resulting velocity mismatch provides opportunities for chondrules formed in previous shock wave events to accrete rims of much smaller grains through collisions. To match speeds with the post-shock gas flow, a chondrule must encounter a mass of gas comparable to its own mass. The gas colliding with the chondrule carries with it some solid grains. Grains much smaller than the chondrule reach their full post-shock number density close behind the shock (Fig. 5B) and collide with the chondrule at maximal relative velocity (Figs. 5 and 6). Particles closer to the chondrule in size have lower number densities and relative speeds. Thus, a chondrule overrun by a shock wave preferentially collides with much smaller particles. Any excess of accreted material on one side of the chondrule would induce rotation of the chondrule (*34*), ensuring roughly concentric buildup of rim material, given a steady supply of fine-grained particles.

The total mass of small particles that collide with a chondrule overrun by a shock wave is about equal to the chondrule's own mass times the dust/gas ratio of the post-shock nebula. That ratio is the same as the pre-shock value for these small particles over most of the distance required for the much larger chondrule to match speeds with the gas. The canonical nebula dust/gas ratio is 0.01. Assuming that the small grains contain a significant fraction of the solid mass (*30*), that their material density is comparable to that of the chondrules, and that they stick efficiently, a chondrule can be expected to accrete about 1% of its own mass in small grains. A 1% change in mass corresponds to a 0.3% change in radius, or the growth of a rim 3 μm thick on a 1-mm chondrule. This result is consistent with the observed thicknesses of fine-grained accretionary rims on chondrules and with the observation that rim thickness is generally proportional to chondrule radius (*35*).

Rim particles accreted immediately behind the shock front (during peak drag heating) may be molten, providing an alternate formation mechanism for the igneous rims discussed above and possibly also for tiny "microchondrules" (*36*). Alternatively, accretion in weaker shock waves or further behind strong shock waves could produce unmelted fine-grained rims.

A concern regarding hypervelocity collisional rim accretion is that high-speed impacts might destroy chondrules. For accretion of rim particles ≲50 μm, however, the chondrule may survive intact, as seen in experimental impacts of millimeter-sized glass spheres at ~5 km s^{-1} into porous targets composed of 50-μm glass beads (*37*). Fine-grained rims on chondrules are com-

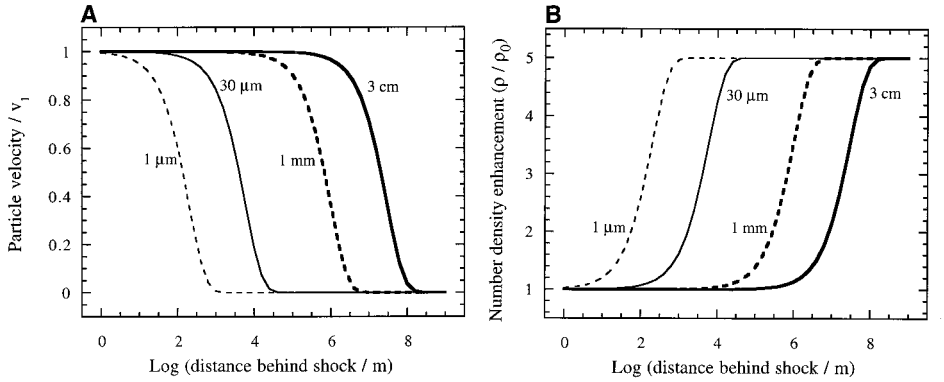

Fig. 5. Relations for particles of density 2 g cm^{-3} overrun by an M 5 shock in a nebula with ambient pressure of 1×10^{-5} atm and ambient temperature of 300 K. (**A**) Velocity with respect to the post-shock gas as a function of distance behind the shock for particles 1 μm, 30 μm, 1 mm, and 3 cm in diameter, normalized to the post-shock gas speed (0.8 times the shock velocity for an M 5 shock). Velocities are approximated by $v = v_0 e^{-x/l_{stop}}$, where v_0 is the initial speed relative to the gas, x is the distance behind the shock, and l_{stop} is the stopping distance in the post-shock gas. The stopping distance is given by $l_{stop} = d_p \rho_p / 2\rho_{gas}$, where d_p is the particle diameter and ρ_p and ρ_{gas} are the particle and gas densities, respectively. For reference, the stopping distances for 1-μm and 1-mm particles in the present case are respectively 200 m and 200 km. The transient velocity sorting of particles according to size is evident. (**B**) Particle number density enhancement relative to the pre-shock value as a function of distance behind the shock for particles 1 μm, 30 μm, 1 mm, and 3 cm in diameter. The asymptotic value is equal to the post- to pre-shock gas density ratio. Particle number densities are temporarily segregated according to size behind the shock.

posed of ~1-μm grains, whose smaller mass would cause even less damage, especially on a hot plastic target rather than a cold brittle one.

Second, the relation of the volatile chemistry of fine-grained matrix and rim material to that of chondrules can also be explained by the shock wave model. One hypothesis is that the fine-grained material is unrelated to chondrules and that the complementary relationship between their volatile chemistries is a coincidence (*2*). Alternatively, fine-grained dust may have been present during chondrule formation and may have acquired the volatiles lost from molten chondrules (*32*). This interpretation requires that dust was present during chondrule formation, that the dust was less strongly heated than the chondrules, and that chondrules and dust heated together eventually became part of the same meteorite.

The latter scenario is consistent with shock wave heating. Fine-grained (micrometer-sized) particles are less strongly heated than chondrules in shock waves because the duration of the drag heat pulse is proportional to particle diameter. Weaker heating of smaller particles implies better retention of volatiles. Furthermore, shock heating will actually facilitate the transfer of volatiles from large particles to smaller ones. A 1-mm chondrule experiences its peak heating and evaporation just behind the shock front, where it is surrounded by micrometer-sized particles that are no longer being drag heated. These smaller grains are therefore cooler and provide a ready substrate for the condensation of volatiles lost from chondrules.

Total gas pressure during chondrule formation. Molten chondrules are unstable and will evaporate under pressures of $\sim 10^{-5}$ bar (the canonical protoplanetary nebula ambient pressure) in a gas of solar composition (*2*, *38*). The rate of evaporation is poorly known (*18*, *39*, *40*). If the time required for a chondrule to evaporate is much longer than the peak heating time, the instability of the liquid does not constrain the environment of chondrule formation. If, however, the evaporation time is shorter than the peak heating time, then the total gas pressure during chondrule formation must have been 10^{-4} to 10^{-3} bar (10 to 100 times the canonical nebula midplane value) in order for chondrule liquids to survive without boiling away (*18*, *38*, *39*). One way to increase the total gas pressure during chondrule formation is to add dust in concentrations up to 500 times that of the overall nebula. The heat of chondrule formation evaporates the dust, producing total gas pressures of 10^{-4} to 10^{-3} bar (*38*).

Alternatively, shock waves strong enough to melt chondrules are naturally accompanied by gas pressure increases of 10 to 74 times the 10^{-5}-bar pre-shock gas pressure (Fig. 2). Therefore, shock wave heating explains both the melting of particles to form chondrules (or the melting of existing chondrules) and the postulated high-pressure environment during their formation.

The f_{O_2} during chondrule formation. Related to pressure is the partial pressure of oxygen, or oxygen fugacity (f_{O_2}), that chondrules experienced during formation (*12*–*14*, *23*, *24*). FeO-poor chondrules must have formed in an environment with an f_{O_2} similar to that of a gas of solar composition [unless the inferred f_{O_2} recorded by chondrules is an artifact of their precursor composition (*24*)], whereas FeO-rich chondrules experienced an f_{O_2} that was four to six orders of magnitude higher (*14*). Variable f_{O_2} has been explained by the evaporation of fine dust in different concentrations (*12*, *38*). In this model, however, the dust concentration required to explain the inferred range of f_{O_2} for each chondrule population is inconsistent with the dust concentration needed to explain the total gas pressure discussed above.

In shock wave heating, however, pressure and f_{O_2} can be independently adjusted by shock compression (which boosts total pressure and f_{O_2} proportionally) (Fig. 2) and by evaporation of concentrated solids (which primarily affects f_{O_2}). Thus, shock wave heating resolves the apparent paradox between f_{O_2} and total pressure during chondrule formation.

Degree of heating and chondrule sizes. Chondrule petrology suggests that larger chondrules were, in general, more strongly heated (at a higher temperature or for longer times or both) than smaller chondrules (*32*). In addition to the possibility that fine-grained dust was less strongly heated than chondrules, fine-grained FeO-poor, DZ, and AO chondrules are typically smaller than other chondrule types. Their textures and, in the case of DZ and AO, their abundant FeS suggest that they were also less strongly heated than other chondrule types (mainly FeO-rich chondrules). We accept this apparent correlation between chondrule size and degree of heating with the caveats that it may be complicated by recycling and that it lacks unequivocal petrologic support. A definitive petrologic correlation between chondrule size and degree of heating would be a key discriminator for the soundness of many chondrule formation mechanisms.

The shock wave model explains the difference in degree of heating experienced by FeO-rich and FeO-poor chondrules. In general, FeO-rich chondrules experienced more heating (*14*) and higher f_{O_2} than FeO-poor chondrules. Stronger shocks produce higher drag heating temperatures, higher postshock total gas pressure, and more particle evaporation, resulting in higher f_{O_2}. Thus, FeO-rich chondrules may be the product of shock waves stronger than those that produced FeO-poor chondrules.

Alternatively, FeO-rich and FeO-poor chondrules may have been formed together. FeO-rich chondrules are generally larger than FeO-poor chondrules (*13*, *14*). Their larger size implies a proportionally longer stopping distance and a longer drag heat pulse duration in the same shock wave (Table 1). The longer drag heat

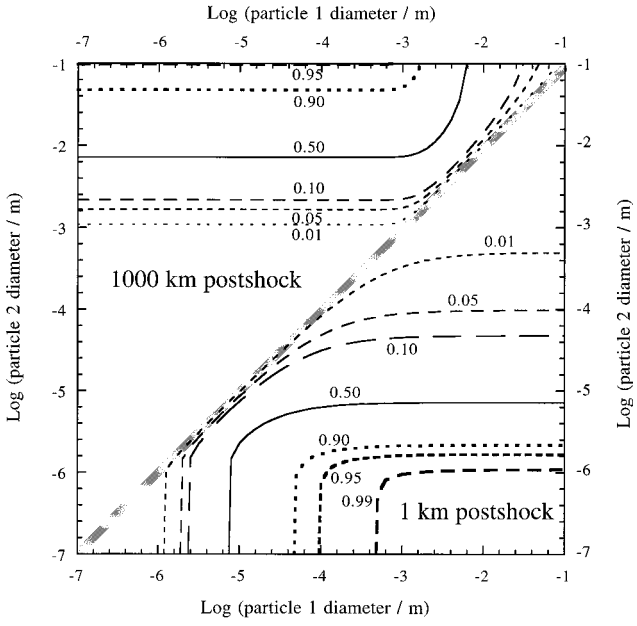

Fig. 6. Contours of mutual particle collision speeds, expressed as a fraction of the post-shock gas velocity v_1 at 1 km (lower right half of plot) and 1000 km (upper left half of plot) behind the shock wave described in the caption of Fig. 5. The logarithms of the diameters of the two collision partners (in meters) define a point on the contour plot from which the mutual collision speed can be estimated. Two different distances can be shown, because the contours for each are symmetric under exchange of the two particle diameters. The figure shows that 1 km behind the shock, a 10-μm particle and a 100-μm particle collide at ~0.35 times the post-shock gas speed; whereas 1000 km behind the shock, a 1-cm particle and a 10-μm particle collide at ~0.60 times the postshock gas speed.

pulse would produce more strongly heated chondrules. In this scenario, the larger FeO-rich chondrules would be more oxidized than FeO-poor chondrules, either because of longer interaction with the post-shock gas or differences in precursor composition.

Formation in localized regions. The relatively rapid heating and slow cooling rates experienced by chondrules constrain their formation to locally hot nebular regions ~100 km or less in thickness (*41*). In addition, there are differences in bulk chemistry and oxygen isotopic composition among chondrules from different meteorites that suggest strongly that the chondrule formation mechanism operated locally and that its products were not mixed throughout the protoplanetary nebula before accreting into asteroids (*12*). The shock wave model satisfies this constraint because the waves' lateral size and the distance they travel (and hence the distance they carry particles) may have almost any value, depending on the mechanism that generates them. The only requirement that the present model levies on the spatial scale of shock waves is that they travel several hundred kilometers, which is far enough to produce the particle heat pulse durations and size-sorting behavior discussed above. This distance easily meets the petrologic constraint that the solids in the protoplanetary nebula not be homogenized before the meteorite parent bodies accreted.

Sources of Nebular Shock Waves

We have shown that shock wave heating agrees with the observed properties of chondrules. As summarized in (*8*), however, strong shock waves dissipate rapidly and their formation requires a great deal of energy (~10% of the energy of gravitational binding to the sun for a chondrule-forming shock at 2 to 3 astronomical units). Thus, it is important to identify a powerful, reliable, repeatable, and astrophysically realistic source for the shock waves. No such source has been positively identified and observed. Although it is beyond the scope of this paper to treat in detail potential shock wave formation mechanisms, we note that four processes capable of creating chondrule-forming shock waves have been treated recently in the literature. These include irregular (clumpy) accretion of interstellar gas onto the protoplanetary nebula (*3*, *7*, *42*), outbursts from the young sun [analogs of FU Orionis events (*3*)], spiral arm instabilities in the disk (*3*, *43*), and eccentric planetesimals moving at hypersonic speeds through the protoplanetary disk (*44*).

REFERENCES AND NOTES

1. D. W. Sears and R. T. Dodd, in *Meteorites and the Early Solar System*, J. F. Kerridge and M. S. Mathews, Eds. (Univ. of Arizona Press, Tucson, AZ, 1988), pp. 3–31.
2. E. Anders and M. Ebihara, *Geochim. Cosmochim. Acta* **46**, 2363 (1989); L. Grossman and J. W. Larimer, *Rev. Geophys. Space Phys.* **12**, 71 (1974).
3. A. P. Boss, in *Chondrules and the Protoplanetary Disk*, R. H. Hewins, R. H. Jones, E. D. R. Scott, Eds. (Cambridge Univ. Press, Cambridge, 1996), pp. 257–64.
4. R. H. Shu, H. Shang, T. Lee, *Science* **271**, 1545 (1997).
5. E. A. King, Ed., *Chondrules and Their Origins* (Lunar and Planetary Institute, Houston, TX, 1983).
6. R. H. Hewins, R. H. Jones, E. D. R. Scott, Eds., *Chondrules and the Protoplanetary Disk* (Cambridge Univ. Press, Cambridge, 1996).
7. L. L. Hood and M. Horanyi, *Icarus* **93,** 259 (1993); L. L. Hood and D. A. Kring, in (*6*), pp. 265–276.
8. J. N. Cuzzi, A. R. Dobrovolskis, R. C. Hogan, in (*6*), pp. 35–44.
9. H. W. Liepmann and A. Roshko, *Elements of Gasdynamics* (Wiley, New York, 1957).
10. T. V. Ruzmaikina and W. H. Ip, *Icarus* **112** 430 (1994); in (*6*), pp. 277–284.
11. S. G. Love and D. E. Brownlee, *Icarus* **89**, 26 (1991).
12. J. N. Grossman, in *Meteorites and the Early Solar System*, J. F. Kerridge and M. S. Mathews, Eds. (Univ. of Arizona Press, Tucson, AZ, 1988), pp. 680–696; H. Nagahara, *Mem. Natl. Inst. Polar Res. Special Issue* **30**, 61 (1984).
13. R. H. Jones and E. R. D. Scott, *Proc. Lunar Planet. Sci. Conf.* **19,** 523 (1989); R. H. Jones, *Geochim. Cosmochim. Acta.* **58**, 5325 (1994); *ibid*. **54**, 1785 (1990); *ibid*. **60**, 3115 (1996); E. R. D. Scott and G. J. Taylor, *Proc. Lunar Planet. Sci. Conf.* **14,** B275 (1983).
14. R. H. Hewins, *Annu. Rev. Earth Planet. Sci*. **25**, 61 (1997).
15. H. C. Connolly Jr., B. D. Jones, R. H. Hewins, *Geochim. Cosmochim. Acta*, in press; R. H. Hewins and H. C. Connolly Jr., in (*6*), pp. 197–204; R. H. Hewins and P. M. Radomsky, *Meteoritics* **25**, 309 (1990); J. P. Greenwood and P. C. Hess, in (*6*), pp. 205–211; G. E. Lofgren, *Geochim. Cosmochim. Acta* **53**, 461 (1989); _____ and W. J. Russell, *ibid.* **50**, 1715 (1986); G. E. Lofgren and A. Lanier, *ibid.* **54**, 3537 (1990); P. M. Radomsky and R. H. Hewins, *ibid.*, p. 3475; G. E. Lofgren, in (*6*), pp. 187–196.
16. Although this lower limit is commonly accepted, the exact values are not firm. Work by R. H. Jones and G. E. Lofgren [*Meteoritics* **28**, 213 (1993)] and S. Weinbruch, H. Buttner, A. Holzheid, M. Roenhauer, and R. H. Hewins [*Meteorit. Planet. Sci.* **33**, 65 (1998)] has begun to place a lower limit between 50° and 10° per hour; however, this research is not definitive. Additional experiments by Y. Yu, R. H. Hewins, and B. Zanda, [in (*6*), pp. 213–19] and Y. Yu and R. H. Hewins (*Geochim. Cosmochim. Acta*, in press) have begun to explore nonlinear cooling rates, which may be more realistic for chondrule formation.
17. Y. Yu, R. H. Hewins, B. Zanda, in (*6*), pp. 213–19; Y. Yu and R. H. Hewins, *Geochim. Cosmochim. Acta*, in press; S. Huang *et al*., *Icarus* **122**, 316 (1996).
18. J. T. Wasson, in (*6*), pp. 45–54.
19. E. R. D. Scott, S. G. Love, A. N. Krot, in (*6*), pp. 87–98.
20. M. K. Weisberg and M. Prinz, in (*6*), pp. 119–127.
21. B. Zanda, Y. Yu, M. Bourot-Denise, R. H. Hewins, *LPI Tech. Rep.* **97–02** (part 1), 68 (1997).
22. J. T. Wasson, *Meteorites, Their Record of Early Solar-System History* (Freeman, New York, 1985).
23. J. A. Wood, *Earth Planet. Sci. Lett.* **70**, 11 (1984).
24. H. C. Connolly Jr., R. H. Hewins, R. D. Ash, B. Zanda, G. E. Lofgren, *Nature* **371**, 136 (1994).
25. P. Hanon, F. Robert, M. Chaussidon, *Meteoritics* **31**, A57 (1996).
26. H. Nagahara, *Nature* **292**, 135 (1981); E. R. Rambaldi, *ibid.* **293**, 558 (1981); R. H. Jones, in (*6*), pp. 163–172; R. H. Jones and L. R. Danielson, *Meteorit. Planet. Sci.* **32**, 753 (1997).
27. C. M. O. Alexander, in (*6*), pp. 233–242.
28. A. N. Krot and J. T. Wasson, *Geochim. Cosmochim. Acta* **59**, 4951 (1995).
29. P. Cassen, in (*6*), pp. 21–28.
30. J. S. Dohnanyi, in *Cosmic Dust*, J. A. M. McDonnell, Ed. (Wiley, New York, 1978), pp. 527–605. A common distribution for a collisionally evolving population is $n(r,r + dr) \propto r^{-3.5}\, dr$, where n is the number of particles per cubic meter with radii between r and $r + dr$.
31. G. E. Lofgren, *Lunar Planet. Sci. Conf*. **28**, 827 (1997); G. E. Lofgren in *LPI Tech. Rep.* **97–02** (part 1), 40 (1997).
32. E. R. D. Scott, D. J. Barber, C. M. Alexander, R. Hutchison, J. A. Peck, in *Meteorites and the Early Solar System*, J. F. Kerridge and M. S. Mathews, Eds. (Univ. of Arizona Press, Tucson, AZ, 1988), pp. 718–745.
33. H. C. Connolly Jr. and R. H. Hewins, *Geochim. Cosmochim. Acta* **59**, 3231 (1995).
34. K. Liffman and M. J. I. Brown, in (*6*), pp. 285–302.
35. J. M. Paque and J. N. Cuzzi, *Lunar. Planet. Sci. Conf*. **28**, 1071 (1997).
36. A. N. Krot and A. E. Rubin, in (6), pp. 181–186.
37. S. G. Love, F. Hörz, D. E. Brownlee, *Icarus* **105**, 216 (1993).
38. D. S. Ebel and L. Grossman, *Lunar Planet. Sci. Conf.* **28,** 317 (1997); D. S. Ebel and L. Grossman, *Meteorit. Planet. Sci*. **32**, A36 (1997); J. A. Wood and A. Hashimoto, *Geochim. Cosmochim. Acta* **57**, 2377 (1993).
39. Y. Yu and R. H. Hewins, *Lunar Planet. Sci. Conf.* **28**, 1613 (1997).
40. A. Hashimoto, *Nature* **347**, 53 (1991).
41. D. L. Sahagian and R. H. Hewins, *Lunar Planet. Sci. Conf*. **23**, 1197 (1992).
42. A. P. Boss and J. A. Graham, *Icarus* **106**, 168 (1993).
43. G. Morfill, H. Spruit, E. H. Levy, in *Protostars and Planets II*, E. H. Levy and J. I. Lunine, Eds. (Univ. of Arizona Press, Tucson, AZ, 1993), pp. 939–978; J. A. Wood, *Meteorit. Planet. Sci.* **31**, 641 (1997).
44. L. L. Hood, *Meteorit. Planet. Sci.* **33**, 97 (1998); S. J. Weidenschilling, F. Marzari, L. L. Hood, *Science* **279**, 681 (1998).

45. We thank P. Cassen, D. Woolum, G. Huss, D. Burnett, T. Ahrens, R. Ash, S. Russell, and R. Jones for their numerous helpful discussions and support on this project. Comments from two anonymous reviews helped to improve this paper. This work was supported by NASA (D. S. Burnett). This is Caltech Division contribution number 8507.